Simple generation of hairless mice for in vivo imaging

doi: 10.1538/expanim.17-0049

Exp. Anim. 66(4), 437–445, 2017

—Original—

Simple generation of hairless mice for *in vivo* imaging

Yoshikazu HOSHINO[1–3)]*, Seiya MIZUNO[1,4)]*, Kanako KATO[1)], Saori MIZUNO-IIJIMA[1)], Yoko TANIMOTO[1)], Miyuki ISHIDA[1)], Noriko KAJIWARA[1)], Tomoki SAKASAI[1,3)], Yoshihiro MIWA[1,4)], Satoru TAKAHASHI[1,4)], Ken-ichi YAGAMI[1,4)], and Fumihiro SUGIYAMA[1,4)]

[1)]*Laboratory Animal Resource Center, University of Tsukuba, 1-1-1 Tennodai, Tsukuba, Ibaraki 305-8575, Japan*
[2)]*Hoshino Laboratory Animals, Inc., 1405 Kouda, Bando, Ibaraki 306-0606, Japan*
[3)]*Doctoral program in Biomedical Sciences, Graduate School of Comprehensive Human Sciences, University of Tsukuba, 1-1-1 Tennodai, Tsukuba, Ibaraki 305-8575, Japan*
[4)]*Faculty of Medicine, University of Tsukuba, 1-1-1 Tennodai, Tsukuba, Ibaraki 305-8575, Japan*

Abstract: The *in vivo* imaging of mice makes it possible to analyze disease progress non-invasively through reporter gene expression. As the removal of hair improves the accuracy of *in vivo* imaging, gene-modified mice with a reporter gene are often crossed with Hos:HR-1 mutant mice homozygous for the spontaneous Hr^{hr} mutation that exhibit a hair loss phenotype. However, it is time consuming to produce mice carrying both the reporter gene and mutant Hr^{hr} gene by mating. In addition, there is a risk that genetic background of the gene-modified mice would be altered by mating. To resolve these issues, we established a simple method to generate hairless mice maintaining the original genetic background by CRISPR technology. First, we constructed the *pX330* vector, which targets exon 3 of *Hr*. This DNA vector (5 ng/μl) was microinjected into the pronuclei of C57BL/6J mice. Induced *Hr* gene mutations were found in many founders (76.1%) and these mutations were heritable. Next, we performed *in vivo* imaging using these gene-modified hairless mice. As expected, luminescent objects in their body were detected by *in vivo* imaging. This study clearly showed that hairless mice could be simply generated by the CRISPR/Cas9 system, and this method may be useful for *in vivo* imaging studies with various gene-modified mice.
Key words: CRISPR/Cas9, hairless, *in vivo* imaging, mouse

Introduction

In vivo molecular imaging is an essential tool for detecting target biomolecules directly and non-invasively, and for visualizing molecular processes. Indocyanine green (ICG) is a common fluorescent molecule used in human medical diagnostics [15]. ICG is a cyanine dye that is removed exclusively by the liver and excreted into the bile [5]. ICG can be excited at 800 nm and emits fluorescence at 840 nm when bound with proteins [2]. Transient overexpression of near-infrared fluorescent protein (iRFP) causes bright fluorescence in cells, tissues, and the entire animal body without the addition of exogenous biliverdin [7]. The iRFP can be excited at 690 nm and emits fluorescence at 713 nm. An optimal fluorescent protein for *in vivo* imaging should have both excitation and emission maxima within a near-infrared window from ~650 nm to 900 nm, for which tissue has the lowest absorbance and less light scattering than at shorter wavelengths [12]. Therefore, iRFP is suitable for deep tissue imaging.

In vivo imaging with the iRFP makes it possible to

(Received 1 May 2017 / Accepted 28 June 2017 / Published online in J-STAGE 18 July 2017)
Address corresponding: F. Sugiyama, Laboratory Animal Resource Center, University of Tsukuba, 1-1-1 Tennodai, Tsukuba, Ibaraki 305-8575, Japan
**These authors contributed equally to this study.*
Supplementary Figures and Tables: refer to J-STAGE: https://www.jstage.jst.go.jp/browse/expanim

detect fluorescent proteins in the living bodies of mice [14]. The hair blocks, absorbs, and scatters light. Especially, Black hair absorbs more light than other color hairs [22, 30]. As even white hair absorbs light, it is very difficult to detect fluorescence signals. Therefore, it is necessary to remove the hair from mice to detect the iRFP signal with *in vivo* imaging system. Nude mice lack hair, although they are immunodeficient [8, 23]. The *FoxN1* gene, located on chromosome 11, is responsible for these phenotypes [4, 21, 29]. *Hr* gene (RefSeq Accession: NM_021877) mutants such as Hos:HR-1 mice also show hair loss without abnormalities in the immune system. These hairless mice are useful for not only skin, immunology, and cancer studies but also *in vivo* imaging [3, 9]. Gene-modified mice are often backcrossed to *Hr* mutant mice for *in vivo* imaging [20]. However, it is time consuming to produce mice carrying both a reporter gene for *in vivo* imaging and mutated *Hr* gene by mating. Moreover, if reporter gene is located on chromosome 14 on which *Hr* gene is located, it is difficult to introduce both mutations by mating. In addition, there is the risk that the genetic background of the reporter mice would be changed by mating.

The CRISPR/Cas9 system is very convenient for inducing specific mutations in various animals. This system is composed of a single guide RNA (sgRNA) and Cas9 protein, which cause site-specific DNA double-strand breaks (DSB), leading to indel mutations by non-homologous end joining (NHEJ) [11, 25]. To shorten the time for producing hairless gene-modified mice and to eliminate the risk of changes in genetic background, we generated hairless mice for *in vivo* imaging using the CRISPR/Cas9 system.

In this study, we tried to produce new hairless mice using the CRISPR/Cas9 system for detecting iRFP signal by *in vivo* imaging.

Materials and Methods

Animals

C57BL/6J and Jcl:CD1 (ICR) mice were purchased from Charles River Laboratories Japan (Kanagawa, Japan) and CLEA Japan (Tokyo, Japan), respectively. The iRFP transgenic mice were generated as described previously [30]. $Hr^{hr/hr}$ mice (RBRC01223) were provided by RIKEN BRC through the National Bio-Resource Project of the MEXT, Japan. Mice were kept in plastic cages under pathogen-free conditions in a room maintained at 23.5 ± 2.5°C and 52.5 ± 12.5% relative humidity under a 14-h light:10-h dark cycle. Mice had free access to commercial chow (MF diet; Oriental Yeast, Tokyo, Japan) and filtered water. All mouse experiments were performed with the approval of the University of Tsukuba Animal Experiment Committee.

Vector construction

The *pX330* plasmid, carrying both gRNA and Cas9 expression units, was a gift from Dr. Feng Zhang (Addgene plasmid 42230) [6]. The oligos, Hr51 CRISPR F (5′-caccAGCCCCTGTGAACGGCATTG-3′) and Hr51 CRISPR R (5′-aaacCAATGCCGTTCACAGGGGCT-3′), were annealed and inserted into the entry site of *pX330* as described previously [18]. The resulting plasmid was designated as *pX330-Hr51*. The oligos, *p2color-Hr51* F (5′-aattAGCCCCTGTGAACGGCATTGTGG-3′) and *p2color-Hr51* R (5′-ggccCCACAATGCCGTTCACAGGGGCT-3′), were annealed and inserted into the entry site of *p2color* vector. This plasmid was designated as *p2color-Hr51*. Transfection into HEK293T cells and fluorescence observations were performed as described previously [18].

Microinjection

Female C57BL/6J mice were injected with pregnant mare serum gonadotropin (PMSG) and human chorionic gonadotropin (hCG) with a 48-h interval, and mated with male C57BL/6J mice. The zygotes were collected from the oviducts. Then, the *pX330-Hr51* DNA vector (circular, 5 ng/μl) was injected into the pronuclei according to standard protocols [10]. The injected embryos (pronuclei stage) were then transferred into pseudopregnant ICR mice.

Genomic PCR and sequence analysis

Screening of founder mice (three weeks old) was performed by PCR using genomic DNA obtained from the tail. The PCR amplicons were passed through MCE-202 MultiNA (Shimadzu, Kyoto, Japan), which is a microchip electrophoresis system for DNA analysis. The off-target effect was examined by PCR and direct sequencing [18]. PCR was performed with AmpliTaq Gold® 360 Master Mix (Applied Biosystems, Foster City, CA) and the primers listed in Supplementary Table 1. The PCR products were purified with a Fast Gene Gel/PCR Extraction Kit, and sequences were analyzed using an Applied Biosystems 3130 Genetic Analyzer (Life Technologies,

Palo Alto, CA) with a BigDye® Terminator v3.1 Cycle Sequencing Kit (Life Technologies).

Imaging of an ICG tube in hairless mice

The ICG tube was detected with an *in vivo* imaging system (IVIS Spectrum; PerkinElmer, Wellesley, MA) and a CT scanner (ALOKA La Theta LCT-100; Hitachi, Tokyo, Japan). All mice were anesthetized with isoflurane. The ICG tube was inserted into the abdominal cavity. Analysis of fluorescence signals was performed with Living Image Software 4.0 (Caliper LifeSciences, Hopkinton, MA). Three-dimensional (3D) reconstruction was performed with OsiriX Lite 7.5 (Pixmeo, Bernex, Switzerland).

Imaging of iRFP embryos

The iRFP fluorescence signal was detected with an *in vivo* imaging system (IVIS Spectrum). The iRFP-expressing embryos at 10.5 days post-coitum (dpc) in the uterus were assessed in female hairless mice crossed with iRFP-expressing male mice. All mice were anesthetized with isoflurane or sacrificed before imaging. The fluorescence signals were analyzed with Living Image Software 4.3.1 (Caliper LifeSciences).

RNA extraction and cDNA synthesis

Total RNA from skin was extracted using Isogen (Nippon Gene Co., Ltd., Tokyo, Japan) in accordance with the manufacturer's instructions. cDNA was synthesized from 5 μg of RNA using Superscript II reverse transcriptase (Thermo Fisher Scientific, San Jose, CA) and oligo (dT) primer (Thermo Fisher Scientific). PCR was performed with AmpliTaq Gold® 360 Master Mix (Applied Biosystems) and the primers listed in Supplementary Table 1. The PCR products were purified with a Fast Gene Gel/PCR Extraction Kit, and sequences were analyzed using an Applied Biosystems 3130 Genetic Analyzer (Life Technologies) with a BigDye® Terminator v3.1 Cycle Sequencing Kit (Life Technologies).

Blood sampling

The blood was sampled at the same time of day (10:00 − 12:00) to control for the chronobiological variability of study parameters. Whole blood samples were taken with a 1-ml syringe and a 26-gauge needle from the caudal vena cava after laparotomy under anesthesia. For hematology analysis, the blood samples (0.1 ml) were placed in 1.5-ml tubes containing Na_2-EDTA (Dojindo Molecular Technologies, Kumamoto, Japan) and analyzed immediately. The remainder of each sample was collected in a 1.5-ml tube for blood chemistry, and the blood was allowed to clot for 30 min and centrifuged (3,000 × g, 5 min) for serum separation. Serum samples were analyzed immediately [13].

Hematology

Hematology analyses were performed using Celltac α (MEK-6458; Nihon Kohden, Tokyo, Japan). The hematological parameters investigated were white blood cell count (WBC), red blood cell count (RBC), hemoglobin concentration (HGB), hematocrit (HCT), mean corpuscular volume (MCV), mean corpuscular hemoglobin (MCH), mean corpuscular hemoglobin concentration (MCHC), and platelet count (PLT). The measurement method was same as previous report [30].

Blood chemistry

Blood chemistry parameters were measured using a Fuji Dri-chem 7000 (Fuji-Film, Tokyo, Japan). The blood chemistry parameters investigated were aspartate aminotransferase, alanine aminotransferase, alkaline phosphatase, blood glucose, blood urea nitrogen, creatinine, total protein, albumin, total bilirubin, calcium, inorganic phosphate, total cholesterol, triglyceride, sodium, potassium, and chloride. The measurement method was same as previous report [30].

Results

Generation of hairless mice by CRISPR/Cas9

To generate hairless mice by the CRISPR/Cas9 system, we first targeted a sequence in the *Hr* gene. According to UCSC Genome Browser, the *Hr* gene located on chromosome 14 has 20 exons. We targeted exon 3, which contains the start codon (Fig. 1). To decrease off-target candidates, we used the CRISPRdirect web server to design CRISPR/Cas guide RNA [19]. The CRISPR target was located 51–73 bp downstream of the start codon of *Hr*. We inserted a 20-bp gRNA target into *pX330*, and the resultant plasmid was designated as *pX330-Hr51*. Next, the cleavage activity of *pX330-Hr51* was examined by the traffic reporter system [11]. The results indicated that *pX330-Hr51* could efficiently cleave the target site (Supplementary Fig. 1B).

We then microinjected 5 ng/μl of the *pX330-Hr51* DNA vector (circular) into the pronuclei of 437 one-cell

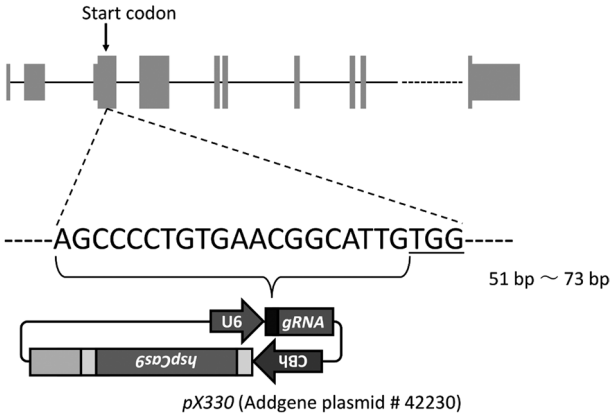

Fig. 1. Schematic for *pX330-Hr51.* The DNA sequence indicate the CRISPR guide RNA target site. The underlined letters indicate the protospacer adjacent motif (PAM) sequence. At the top of this figure, thin gray boxes indicate untranslated regions. Thick gray boxes indicate coding sequence regions.

stage embryos obtained from C57BL/6J mice. No morphological abnormalities were observed in 395 of 437 one-cell embryos immediately after microinjection. These one-cell embryos with a normal appearance were transferred into the oviducts of pseudopregnant recipient ICR mice, and 88 neonates, including six without hair, were obtained. The hairless phenotype caused by *Hr* mutation was inherited in a recessive manner. Therefore, we confirmed *Hr* gene mutation even in founders with hair. The heteroduplex mobility assay (HMA) with MultiNA revealed indel mutations in 67 of 88 mice, including six with no hair (Table 1).

To determine whether the *pX330-Hr51* DNA vector was integrated into the chromosomes, we performed PCR with founder mouse genomic DNA and a primer pair for Cas9 detection. PCR products were detected in four founder mice (Table 1). Therefore, we succeeded in generating 63 (including five hairless) mutant mice without insertion of *pX330*. In the mice carried *pX330-Hr* chromosomal integration, ubiquitously expression of the gRNA for *Hr* and Cas9 may result in accumulating the off-target mutations in each somatic and germ cells. Therefore, we refrained from using them. In addition, off-targets of one male hairless founder were checked and no mutations were found (Supplementary Table 4).

Inheritance and gene expression

To confirm the hereditary and mutant sequence detail, male hairless founder #70 was crossed with a female wild-type mouse (Fig. 2A). We obtained 11 F_1 mice with hair. Unexpectedly, three types of mutations were detected in these animals: Δ2 (TT deletion), Δ5 (CGGCA deletion), and +1 (A insertion) (Fig. 2B). The mice carrying the same mutation sequence were intercrossed and all F_2 homozygous mutants were hairless. As no different phenotypes were found among them, we used the Δ5 hairless mouse line and their mutant allele was named Hr^{em1Utr}.

We also investigated the *Hr* RNA expression and its sequence from $Hr^{em1Utr/em1Utr}$ and $Hr^{hr/hr}$ mice. The $Hr^{hr/hr}$ mouse strain showed the hairless phenotype caused by spontaneous insertion mutation in intron 7 of the *Hr* gene, and has already been widely used in *in vivo* studies. The total RNAs of homozygous mutant skin were collected and RT-PCR was performed with three primer pairs (exon 3 to exon 4, exon 7 to exon 12, and exon 13 to exon 19). PCR products were detected under all conditions (Figs. 3B–3D). We then confirmed the sequences of these RT-PCR products and detected the CRISPR-induced 5-bp deletion mutation in $Hr^{em1Utr/em1Utr}$ mouse cDNA (Fig. 2B). The results indicated that the CRISPR-induced heritable genetic mutation resulted in mutant RNA expression and hairless phenotype.

Hairless phenotype

We then confirmed that temporal changes in the hairless mouse phenotype in $Hr^{em1Utr/em1Utr}$ mice (Fig. 4 and

Table 1. Generation of CRISPR/Cas9-mediated *Hr* mutant mice

Injected DNA	Oocytes injected	Oocytes transferred	Number of newborns		Number of newborns without insertion of *pX330*
pX330-Hr51 (5 ng/μl)	437	395	Mutated and hairless	6 (6.8 %)[a]	5
			Mutated	61 (69.3 %)[b]	58
			Wild-type	21 (23.9 %)[c]	21
			Sum	88	84 (95.5 %)[d]

[a]Mutated and hairless/ Sum of newborns. [b]Mutated newborns/ Sum of newborns. [c]Wild-type newborns/ Sum of newborns. [d]Newborns without insertion of *pX330*/ Sum of newborns.

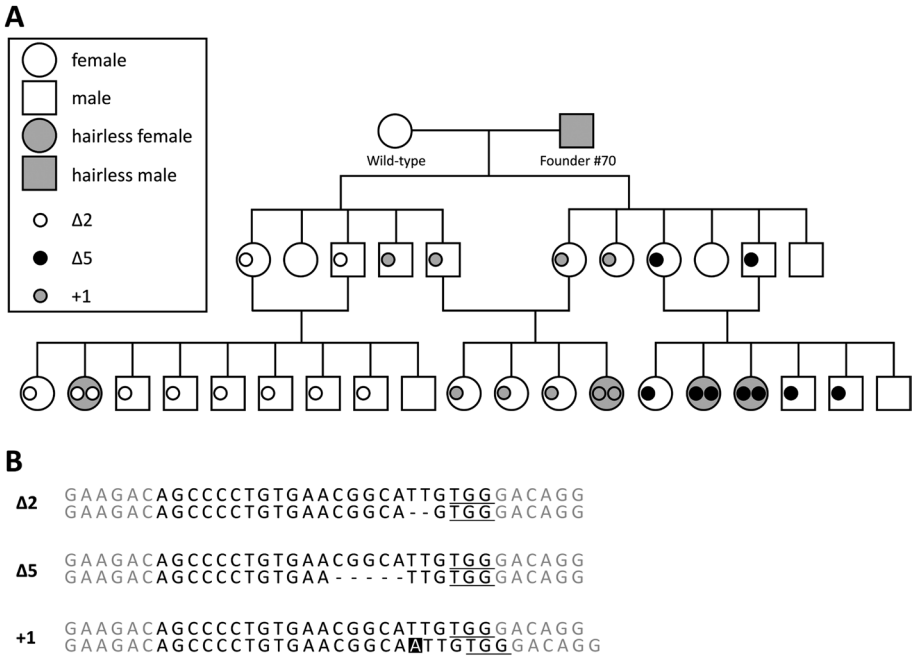

Fig. 2. Pedigree of founder #70 line. (A) Circles and squares represent female and male mice, respectively. The gray circles and squares represent hairless phenotypes. The small white, black, and gray circles indicate 2-bp deletion, 5-bp deletion, and 1-bp insertion alleles, respectively. (B) There were three types of mutation in the founder #70 line. The hyphens indicate deletion. The white letter indicates insertion.

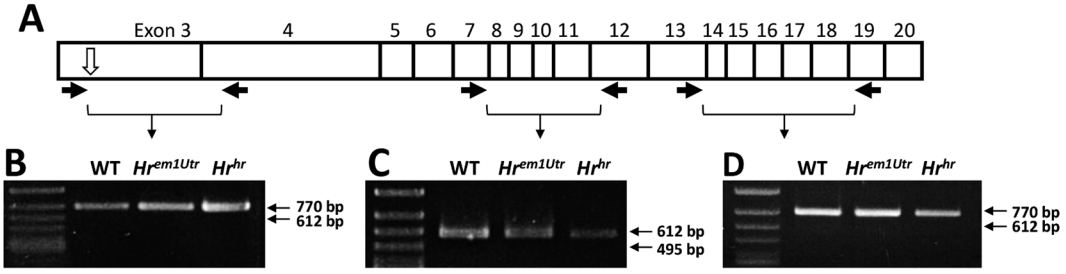

Fig. 3. Reverse transcription PCR of wild-type, $Hr^{em1Utr/em1Utr}$, and $Hr^{hr/hr}$ mice. (A) Schematic for reverse transcription PCR. The white arrow indicates the deletion region. The black arrows indicate primers. (B) The PCR products of 755 bp from exon 3 to exon 4, (C) 588 bp from exon 7 to exon 12, and (D) 760 bp from exon 13 to exon 19 are shown to demonstrate the presence of cDNA. WT, wild-type mice; Hr^{em1Utr}, $Hr^{em1Utr/em1Utr}$ mice; Hr^{hr}, $Hr^{hr/hr}$ mice.

Supplementary Fig. 2A) and $Hr^{hr/hr}$ mice (Supplementary Figs. 2B and 2C). First, $Hr^{em1Utr/em1Utr}$ mice lost their ventral hair at 4 weeks of age. Next, the hair loss progressive from the ventral side to the dorsal side in 2–4 weeks (Fig. 4 and Supplementary Fig. 2A). In contrast, the hair loss in $Hr^{hr/hr}$ mice started at 2 weeks of age [26]. It progressed rapidly from the rostral to the caudal side and $Hr^{hr/hr}$ mice were completely hairless by 4 weeks of age (Supplementary Figs. 2B and 2C) [28]. The $Hr^{em1Utr/em1Utr}$ mice grew slowly compared with wild-type controls (Supplementary Fig. 3). However, there was no difference in weight after 7 weeks of age. In hematology and blood chemistry analyses, we found minor differences related to red blood cells (Supplementary Table 2 and 3). This phenotype was consistent with $Hr^{hr/hr}$ mice [24, 27].

In vivo imaging of $Hr^{em1Utr/em1Utr}$ mice with ICG tube implantation

To confirm whether $Hr^{em1Utr/em1Utr}$ mice are available

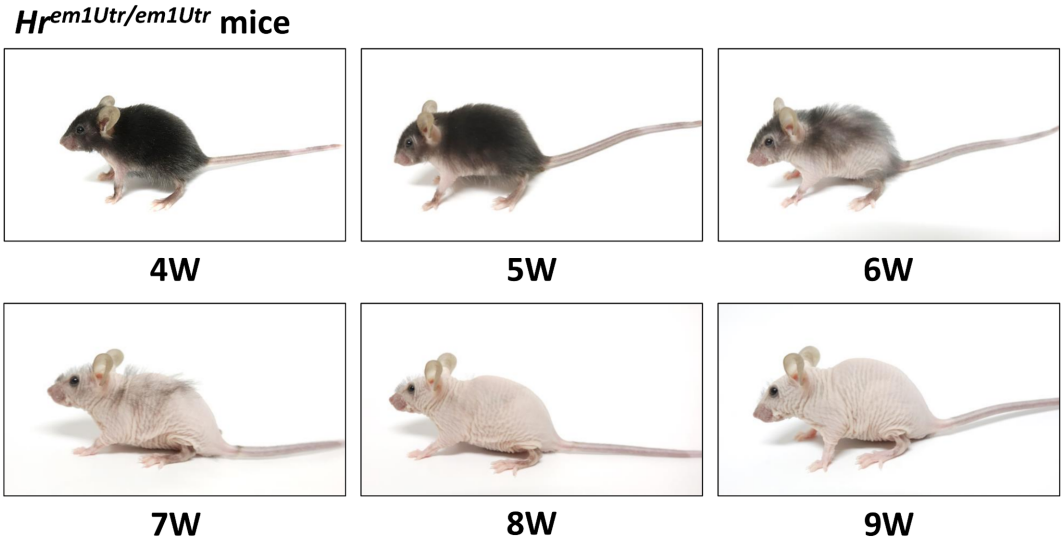

Fig. 4. Temporal changes in $Hr^{em1Utr/em1Utr}$ mice. Female $Hr^{em1Utr/em1Utr}$ mice lost ventral hair at 4 weeks of age. After 6 weeks of age, they gradually lost dorsal hair.

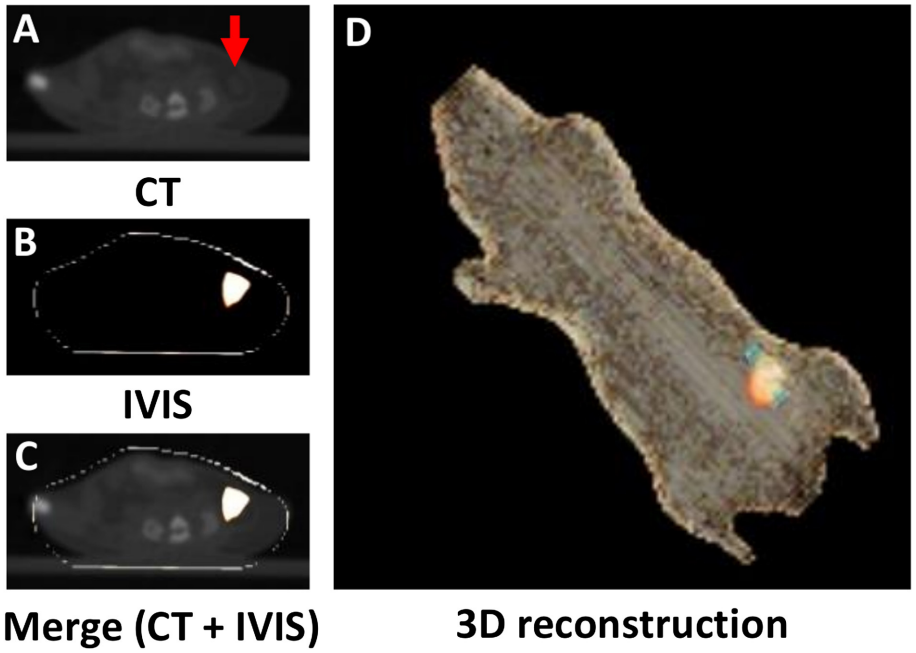

Fig. 5. *In vivo* imaging of $Hr^{em1Utr/em1Utr}$ mice with ICG tube implantation. (A) CT plane. The arrow indicates ICG tube. (B) IVIS plane. (C) Merge (CT + IVIS). (D) 3D reconstruction of merge by OsiriX Imaging Software. Orange light indicates fluorescence signal. Blue light indicates ICG tube. The ICG tube was easily identified using an IVIS Spectrum *in vivo* imaging system equipped with 745 nm excitation and 820 nm emission filters.

for *in vivo* imaging, ICG-filled artificial tubes were implanted into the abdominal cavity of $Hr^{em1Utr/em1Utr}$ mice. The tubes and fluorescence signals were detected by CT and IVIS, respectively. The position of the tube was consistent with that of ICG fluorescence (Figs. 5A–D). These results indicated that the ICG fluorescence could be easily detected in the abdominal cavity of $Hr^{em1Utr/em1Utr}$ mice.

To confirm whether $Hr^{em1Utr/em1Utr}$ mice are available for detecting vital iRFP, female $Hr^{em1Utr/em1Utr}$ mice were

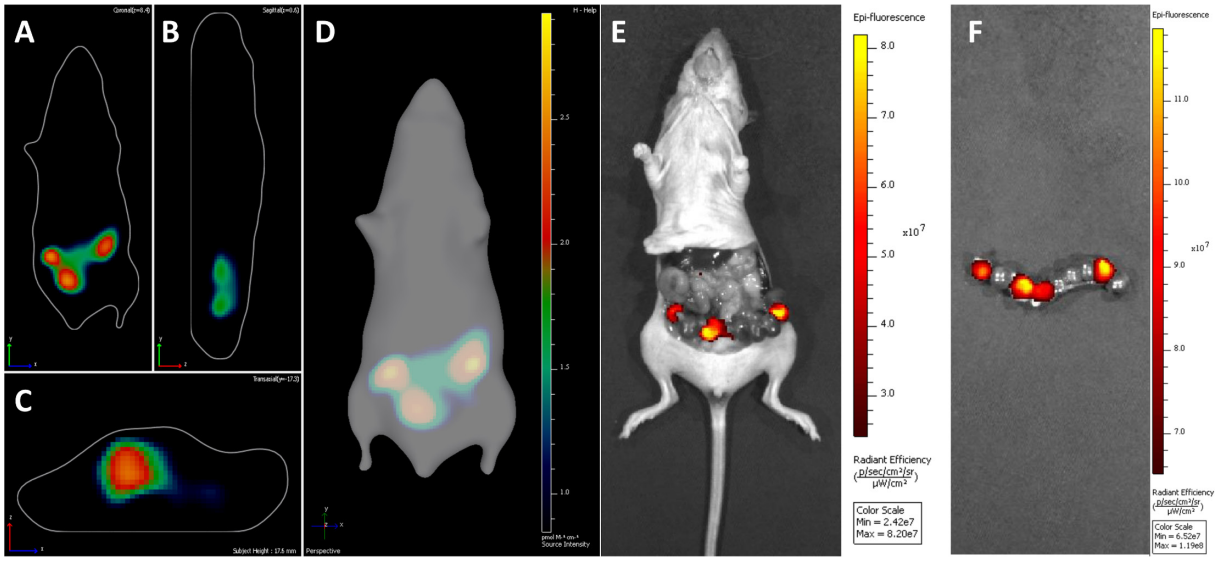

Fig. 6. *In vivo* imaging of $Hr^{em1Utr/em1Utr}$ mice crossed with iRFP transgenic mice. (A) Coronal plane. (B) Sagittal plane. (C) Transverse plane. (D) 3D reconstruction of diffuse luminescence imaging tomography. (E), (F) Uterus after celiotomy. iRFP expression in embryos (10.5 dpc) was identified using an IVIS Spectrum *in vivo* imaging system equipped with 675 nm excitation and 720 nm emission filters.

crossed with iRFP-expressing male mice. The iRFP-expressing embryos in the uterus were detected at 10.5 dpc. The embryos with iRFP signals were detected in the coronal plane (Fig. 6A), the sagittal plane (Fig. 6B), and transverse plane (Fig. 6C). On 3D reconstruction of diffuse luminescence imaging tomography, three embryos expressing iRFP were detected (Fig. 6D). After celiotomy, the positions of iRFP-expressing embryos were almost consistent with those of iRFP fluorescence in 3D reconstruction (Fig. 6E). However, four rather than three embryos expressing iRFP were present in the uterus of the $Hr^{em1Utr/em1Utr}$ mouse (Fig. 6F). These results indicated that the iRFP-expressing embryos could be detected in the uterus of $Hr^{em1Utr/em1Utr}$ mice.

Discussion

Using the CRISPR/Cas9 system, we generated a novel hairless mouse strain designated as $Hr^{em1Utr/em1Utr}$ mice. The complete hair loss in this mouse strain permitted *in vivo* imaging with ICG and iRFP. Although minor abnormalities were found in red blood cells of this mouse strain in comparison with Hr^{hr} mice [24, 27], there were no major abnormal phenotypes that prevented the normal biological activity and long-term *in vivo* imaging studies. These results indicated that the hairless mice generated by CRISPR/Cas9 were useful for *in vivo* imaging.

It is necessary to remove hair from mice before *in vivo* imaging, because hair blocks, absorbs, and scatters light. There are several ways to remove the hair without the need for genetic modification. Shaving with a razor can be performed easily to remove the hair, but is associated with a risk of scab formation due to bleeding, which also block, absorb, and scatter light. Depilatory cream is also used, but this takes time. Especially, 3D *in vivo* imaging requires removal of hair from the whole body. In contrast, *Hr* mutant hairless mice make it possible to begin *in vivo* imaging immediately without removal of hair. This benefit becomes significant when many mice must be used or *in vivo* imaging must be repeated many times.

In general, female $Hr^{hr/hr}$ mice often fail to nurse their litters due to abnormal lactation. Although outbred female $Hr^{hr/hr}$ mice, such as Hos:HR-1 hairless mice, can nurse their litters, $Hr^{hr/hr}$ mice with the C57BL/6JJcl genetic background often fail to nurse their litters. In this study, female $Hr^{em1Utr/em1Utr}$ mice also failed to nurse their litters. Therefore, our observations support the suggestion that this low nursing activity is dependent on the genetic background [28].

Although the mechanism by which *Hr* mutations cause hair loss is not completely understood at the molecular level [16], several *Hr* mutant mouse stains have been reported. Null *Hr* mice ($Hr^{-/-}$), generated by gene targeting, showed both hair loss and severe wrinkling of the

skin [31]. In this strain, the genomic region containing exons 7–11 of *Hr* was deleted and there was no expression of *Hr* mRNA or Hr protein. The $Hr^{rh\text{-}8j}$ spontaneous mutant strain also showed both hair loss and wrinkling of the skin. This mutant carried a nonsense mutation of GA-to-TT substitution at positions 1,910 and 1,911 in exon 5 of *Hr* [1]. As $Hr^{rh\text{-}8j}$ mutant mRNA may be degraded by nonsense-mediated mRNA decay (NMD), small amounts of mutant mRNA were detected in their skin [31]. In contrast, $Hr^{hr/hr}$ mice did not show wrinkling of the skin but did show hair loss. The Hr^{hr} allele has a spontaneous retroviral insertion (approximately 13 kb) into intron 7 [28]. Both wild-type *Hr* mRNA and two additional long mRNAs were expressed from this allele [31]. These additional long mRNAs may arise from aberrant splicing and act in a dominant negative manner to cause the observed loss of hair. These previous reports suggested that *Hr* null mutation yields both hair loss and severe wrinkling of the skin. Conversely, partial inhibition of *Hr* leads to hair loss but not to wrinkling of the skin. Interestingly, $Hr^{hr/hr}$ mice showed complete hair loss and very mild wrinkling of the skin. In addition, mutant Hr^{em1Utr} mRNA was not degraded (Figs. 3B–3D). The CRISPR target sequence was designed according to exon 3 of *Hr* and a 5-bp deletion was induced within its target site. This deletion may induce a frameshift mutation with a stop codon in exon 3 (Supplementary Fig. 4A). In theory, this mutant mRNA should be degraded by NMD. However, there was no difference in the expression level of this mRNA between wild-type and $Hr^{em1Utr/em1Utr}$ mice (Fig. 3). These data suggest that an in-frame ATG, other than the original start codon, functions as an illegitimate start codon and an N-terminal truncated Hr protein results in the phenotype with hair loss and very mild wrinkling of the skin (Supplementary Figs. 4A and 4B). Thus, such as truncated protein which was induced by indel mutation was reported from another group [17]. On the other hands, there is also a possibility that this phenotypic difference is depended on genetic background because those of $Hr^{hr/hr}$ and $Hr^{em1Utr/em1Utr}$ mice are C57BL/6JJcl and C57BL/6J, respectively.

Although three iRFP-expressing embryos were identified in 3D reconstruction of diffuse luminescence imaging tomography (Fig. 6D), four iRFP-expressing embryos were identified in the uterus after celiotomy (Fig. 6F). In fact, our results indicated that it is difficult to distinguish adjacent iRFP-expressing embryos (10.5 dpc). In late pregnancy, it may be possible to distinguish adjacent iRFP-expressing embryos. Further studies are required to establish the method for analyzing the embryos *in utero* from implantation to perinatal stage.

In conclusion, we generated a novel hairless mouse strain, $Hr^{em1Utr/em1Utr}$, using CRISPR/Cas9. These hairless mice enabled the *in vivo* imaging with ICG tubes and iRFP transgenic mice. The CRISPR/Cas9 system could be useful for generating genetically modified hairless mice for *in vivo* imaging studies.

Conflict of Interest

The authors declare there are no conflicts of interest.

Acknowledgments

This work was supported by JSPS KAKENHI Grant Number JP26221004, JP15H04281, JP16K14589, and JP16H01630. We thank the members of the Sugiyama Laboratory for helpful discussions and encouragement.

References

1. Ahmad, W., Panteleyev, A.A., Sundberg, J.P., and Christiano, A.M. 1998. Molecular basis for the rhino ($hr^{rh\text{-}8J}$) phenotype: a nonsense mutation in the mouse hairless gene. *Genomics* 53: 383–386. [Medline] [CrossRef]
2. Arichi, N., Mitsui, Y., Ogawa, K., Nagami, T., Nakamura, S., Hiraoka, T., Yasumoto, H., and Shiina, H. 2014. Intraoperative fluorescence vascular imaging using indocyanine green for assessment of transplanted kidney perfusion. *Transplant. Proc.* 46: 342–345. [Medline] [CrossRef]
3. Benavides, F., Oberyszyn, T.M., VanBuskirk, A.M., Reeve, V.E., and Kusewitt, D.F. 2009. The hairless mouse in skin research. *J. Dermatol. Sci.* 53: 10–18. [Medline] [CrossRef]
4. Byrd, L.G. 1993. Regional localization of the nu mutation on mouse chromosome 11. *Immunogenetics* 37: 157–159. [Medline] [CrossRef]
5. Chang, C.C., Huang, H.C., Liu, K.L., Wu, Y.M., Lee, J.J., Jiang, S.F., and Su, M.Y. 2016. Clinical feasibility of Gd-EOB-DTPA-enhanced MR imaging for assessing liver function: validation with ICG tests and parenchymal cell volume. *Clin. Imaging* 40: 797–800. [Medline] [CrossRef]
6. Cong, L., Ran, F.A., Cox, D., Lin, S., Barretto, R., Habib, N., Hsu, P.D., Wu, X., Jiang, W., Marraffini, L.A., and Zhang, F. 2013. Multiplex genome engineering using CRISPR/Cas systems. *Science* 339: 819–823. [Medline] [CrossRef]
7. Filonov, G.S., Piatkevich, K.D., Ting, L.M., Zhang, J., Kim, K., and Verkhusha, V.V. 2011. Bright and stable near-infrared fluorescent protein for *in vivo* imaging. *Nat. Biotechnol.* 29: 757–761. [Medline] [CrossRef]
8. Flanagan, S.P. 1966. 'Nude', a new hairless gene with pleio-

tropic effects in the mouse. *Genet. Res.* 8: 295–309. [Medline] [CrossRef]
9. Fujii, M., Endo-Okuno, F., Iwai, A., Doi, K., Tomozawa, J., Kohno, S., Inagaki, N., Nabe, T., and Ohya, S. 2016. Hypomorphic mutation in the hairless gene accelerates pruritic atopic skin caused by feeding a special diet to mice. *Exp. Dermatol.* 25: 565–567. [Medline] [CrossRef]
10. Gordon, J.W. and Ruddle, F.H. 1981. Integration and stable germ line transmission of genes injected into mouse pronuclei. *Science* 214: 1244–1246. [Medline] [CrossRef]
11. Hasegawa, Y., Hoshino, Y., Ibrahim, A.E., Kato, K., Daitoku, Y., Tanimoto, Y., Ikeda, Y., Oishi, H., Takahashi, S., Yoshiki, A., Yagami, K., Iseki, H., Mizuno, S., and Sugiyama, F. 2016. Generation of CRISPR/Cas9-mediated bicistronic knock-in ins1-cre driver mice. *Exp. Anim.* 65: 319–327. [Medline] [CrossRef]
12. Jöbsis, F.F. 1977. Noninvasive, infrared monitoring of cerebral and myocardial oxygen sufficiency and circulatory parameters. *Science* 198: 1264–1267. [Medline] [CrossRef]
13. Khokhlova, O.N., Tukhovskaya, E.A., Kravchenko, I.N., Sadovnikova, E.S., Pakhomova, I.A., Kalabina, E.A., Lobanov, A.V., Shaykhutdinova, E.R., Ismailova, A.M., and Murashev, A.N. 2017. Using Tiletamine-Zolazepam-Xylazine Anesthesia Compared to CO2-inhalation for Terminal Clinical Chemistry, Hematology, and Coagulation Analysis in Mice. *J. Pharmacol. Toxicol. Methods* 84: 11–19. [Medline] [CrossRef]
14. Lai, C.W., Chen, H.L., Yen, C.C., Wang, J.L., Yang, S.H., and Chen, C.M. 2016. Using Dual Fluorescence Reporting Genes to Establish an *In Vivo* Imaging Model of Orthotopic Lung Adenocarcinoma in Mice. *Mol. Imaging Biol.* 18: 849–859. [Medline] [CrossRef]
15. Landsman, M.L., Kwant, G., Mook, G.A., and Zijlstra, W.G. 1976. Light-absorbing properties, stability, and spectral stabilization of indocyanine green. *J. Appl. Physiol.* 40: 575–583. [Medline]
16. Liu, Y., Sundberg, J.P., Das, S., Carpenter, D., Cain, K.T., Michaud, E.J., and Voy, B.H. 2010. Molecular basis for hair loss in mice carrying a novel nonsense mutation ($Hr^{rh\text{-}R}$) in the hairless gene (*Hr*). *Vet. Pathol.* 47: 167–176. [Medline] [CrossRef]
17. Makino, S., Fukumura, R., and Gondo, Y. 2016. Illegitimate translation causes unexpected gene expression from on-target out-of-frame alleles created by CRISPR-Cas9. *Sci. Rep.* 6: 39608. [Medline] [CrossRef]
18. Mizuno, S., Dinh, T.T., Kato, K., Mizuno-Iijima, S., Tanimoto, Y., Daitoku, Y., Hoshino, Y., Ikawa, M., Takahashi, S., Sugiyama, F., and Yagami, K. 2014. Simple generation of albino C57BL/6J mice with G291T mutation in the tyrosinase gene by the CRISPR/Cas9 system. *Mamm. Genome* 25: 327–334. [Medline] [CrossRef]
19. Naito, Y., Hino, K., Bono, H., and Ui-Tei, K. 2015. CRISPRdirect: software for designing CRISPR/Cas guide RNA with reduced off-target sites. *Bioinformatics* 31: 1120–1123. [Medline] [CrossRef]
20. Nakanishi, T., Kokubun, K., Oda, H., Aoki, M., Soma, A., Taniguchi, M., Kazuki, Y., Oshimura, M., and Sato, K. 2012. Bioluminescence imaging of bone formation using hairless osteocalcin-luciferase transgenic mice. *Bone* 51: 369–375. [Medline] [CrossRef]
21. Nehls, M., Pfeifer, D., Schorpp, M., Hedrich, H., and Boehm, T. 1994. New member of the winged-helix protein family disrupted in mouse and rat nude mutations. *Nature* 372: 103–107. [Medline] [CrossRef]
22. Ozeki, H., Ito, S., Wakamatsu, K., and Thody, A.J. 1996. Spectrophotometric characterization of eumelanin and pheomelanin in hair. *Pigment Cell Res.* 9: 265–270. [Medline] [CrossRef]
23. Pantelouris, E.M. 1968. Absence of thymus in a mouse mutant. *Nature* 217: 370–371. [Medline] [CrossRef]
24. Reske-Kunz, A.B., Scheid, M.P., and Boyse, E.A. 1979. Disproportion in T-cell subpopulations in immunodeficient mutant *hr/hr* mice. *J. Exp. Med.* 149: 228–233. [Medline] [CrossRef]
25. Singh, P., Schimenti, J.C., and Bolcun-Filas, E. 2015. A mouse geneticist's practical guide to CRISPR applications. *Genetics* 199: 1–15. [Medline] [CrossRef]
26. Sundberg, J.P. and King, L.E. Jr. 2001. Morphology of hair in normal and mutant laboratory mice. *Eur. J. Dermatol.* 11: 357–361. [Medline]
27. Suzu, S., Tanaka-Douzono, M., Nomaguchi, K., Yamada, M., Hayasawa, H., Kimura, F., and Motoyoshi, K. 2000. p56(dok-2) as a cytokine-inducible inhibitor of cell proliferation and signal transduction. *EMBO J.* 19: 5114–5122. [Medline] [CrossRef]
28. Suzuki, O., Koura, M., Noguchi, Y., Uchio-Yamada, K., and Matsuda, J. 2013. Zygosity determination in hairless mice by PCR based on *Hr*(*hr*) gene analysis. *Exp. Anim.* 62: 267–273. [Medline] [CrossRef]
29. Takahashi, Y., Shimizu, A., Sakai, T., Endo, Y., Osawa, N., Shisa, H., and Honjo, T. 1992. Mapping of the nu gene using congenic nude strains and in situ hybridization. *J. Exp. Med.* 175: 873–876. [Medline] [CrossRef]
30. Tran, M.T., Tanaka, J., Hamada, M., Sugiyama, Y., Sakaguchi, S., Nakamura, M., Takahashi, S., and Miwa, Y. 2014. *In vivo* image analysis using iRFP transgenic mice. *Exp. Anim.* 63: 311–319. [Medline] [CrossRef]
31. Zarach, J.M., Beaudoin, G.M. 3rd., Coulombe, P.A., and Thompson, C.C. 2004. The co-repressor hairless has a role in epithelial cell differentiation in the skin. *Development* 131: 4189–4200. [Medline] [CrossRef]